ISSN:2790-1688 DOI: 10.56028/aetr.2.1.443

Insights into the mechanism of g-C_3N_4@a-Fe_2O_3 microsphere heterogeneous activation of hydrogen peroxide under visible light

Jingwei Chen

Ministry of Education Key Laboratory of Integrated Regulation and Resource Development on Shallow Lakes, Hohai University, Nanjing 210098, PR China

College of Environment, Hohai University, Nanjing 210098, PR China

1914050123@hhu.edu.cn (Jingwei Chen, Tel: +86 19850419185)

Abstract. A-Fe_2O_3 complex g-C_3N_4@a-Fe_2O_3 was successfully prepared by solvothermal method and used in optical Fenton photocatalytic process. Using experimental instruments such as XPS, XRD, DRS, TEM, FTIR, and photochemistry to characterize composite materials. According to the mechanism of the photocatalytic process, combining A-Fe_2O_3/H_2O_2 Fenton reagent with g-C_3N_4 photocatalyst under visible light conditions can effectively accelerate the mineralization of pollutants. The photocatalytic performance of g-C_3N_4@a-Fe_2O_3 were evaluated by the decomposition of bisphenol A. When the content of a-Fe_2O_3 is 15%, the photocatalytic efficiency of the composite is the highest. In addition, cyclic operation, iron leaching concentration, fresh and XRD pattern studies indicate that g-C_3N_4@a-Fe_2O_3 composites are very stable and reusable. The results show that the decomposition of BPA by persulfate is a non-free radical reaction, but the coupling a-Fe_2O_3 with g-C_3N_4 can effectively activate the formation of persulfate free radicals and reduce BPA under visible light radiation. Studies showed that free radicals generated by electron holes and persulfate formed on catalysts were the main causes of BPA decomposition. Therefore, combined with previous research results, this paper proposed the mechanism of g-C_3N_4@a-Fe_2O_3 composite photocatalytic reaction by photo-Fenton. More importantly, this work demonstrates a novel approach to activate persulfates that can efficiently degrade pops and gives some new ideas on the remediation of persulfates in contaminated Water.

Keywords: g-C_3N_4@a-Fe_2O_3; Fenton photocatalytic process; persulfates; non-free radical reaction

1. Introduction

Due to their benefits of purity, energy efficiency, safety, and the absence of secondary pollution, AOH_2O_2 based on the generation of reactive oxygen species, such as the Fenton reaction, photocatalytic oxidation, ozonation, etc., are regarded as efficient methods of degradation of harmful organic (and occasionally inorganic) pollutants in wastewater2, 3. As a result, numerous studies have been conducted in an effort to increase the treatment AOH_2O_2 efficiency of AOH_2O_2, lower pollution, and improve performance. Heterogeneous is more of a worry than homogeneous AOH_2O_2 due to its moderate reaction conditions and essentially nonexistent post-reaction sludge production4, 5.

Polymeric graphite-like carbon nitride (g-C_3N_4), developed recently, has a moderately dense strip energy (~2.7 eV), a low cost, strong chemical and thermal durability, a straightforward synthesis procedure, and a two-dimensional metal-free structure with just carbon and nitrogen. It is a potentially useful solar photocatalytic substance6, 7. In contrast, the majority of metal oxide photocatalysts release poisonous metal ions and only can utilize ultraviolet light to generate conductive band electrons (e-) and valence band holes (h+) that can be used to degrade pollutants. Graphite carbon nitride (g-C_3N_4), which only contains carbon and nitrogen, has been utilized in a number of photocatalytic applications9-11 under visible light to reduce environmental concerns and increase solar energy productivity. The polymeric semiconductor exhibits an intrinsic visible light response and is low-cost, very stable, and environmentally benign12.

Iron oxide (a-Fe_2O_3) is abundant in earth's surface soils, sediments, rocks, and water13. Due to its non-toxicity, low cost, availability and corrosion resistance, goethite (a-Fe_2O_3) has been widely

ISSN:2790-1688 DOI: 10.56028/aetr.2.1.443
used in rechargeable lithium-ion batteries, body sensing applications, organic pollutant degradation, water purification, magnetic components, electrode materials and other applications14-16. Many fellows have prepared manifold forms of a-Fe_2O_3, such as nanorods, sea urchins, nanospheres, arrays, and pancakes, and have assessed their photocatalytic activity17-19. Although exhibits high absorption capacity in the visible spectrum's reddish spectrum (1.9-2.2 eV), charge carrier recombination reduces the efficiency of a-Fe_2O_3 as a photocatalyst. However, the drawback of pure g-C_3N_4 is its limited specific surface area and high rate of photoinduced charge recombination6.

As a result, modifications are needed to dispel these inherent defects. The functionalization of metal nanoparticles20, 21, adulteration of metal$_{20}$ and non-metal components, increase of specific surface area21, 22, development of composite materials and heterostructures23-29, and control of shape are actions taken to improve the photocatalytic activity of g-C_3N_4 30-32. Additionally, it has been demonstrated that the characteristics of the organic precursors as well as the actual heat treatment conditions (such as temperature, atmosphere) utilized to generate g-C_3N_4 affect the activity of such photocatalysts (melamine, urea, etc.) 33-35. Therefore, different routes can prepare materials with various catalytic activities. linking with other semiconductors is of particular interest among the different approaches to improving g-C_3N_4 activity. The coupling of different semiconductors and nanocomposites is an desired development of inexpensive materials with advanced performance. It is formed on the basis of abundant raw materials and can show distinctive performance not reflected in personal compound materials. Pure g-C_3N_4's photocatalytic activity can be enhanced by recombination of g-C_3N_4 with different metal oxides to enhances the e~/h+ separation effect and speeds up visible light absorption23, 24, 36-38. The strategy is to effectively separate photocarriers by choosing oxides with energy-matched conductance (CB) and valence band (VB) for g-C_3N_4, and is capable of controlling the separation and transfer of charges. Although H_2O_2 can produce $SO_4^{\cdot-}$ through ultraviolet radiation and thermal activation, the use of these techniques in practical applications is rather limited due to the high energy input required.36, 37 In recent years, transition excessive metals have been used to activate H_2O_2 to degrade contaminants in water38, of which iron (usually dissolved Fe_2+) is widely used due to its non-toxic, abundant and effective properties39-42. However, because ferrous iron is inactivated due to rapid oxidation and deposition into ferrous iron, it also increases the operating costs of removing iron sludge from water for purification after reaction.

Although iron oxides exhibit good properties under laboratory conditions, leaching of harmful iron ions may have harmful side effects in industrial applications43. Therefore, in order to use iron based AOH_2O_2 for wastewater treatment, it is necessary to determine the mechanism of Fe_2O_3 activation AOH_2O_2 process and solve the problem of side effects. One concept is to use the high catalytic capacity of a-Fe_2O_3 and the photocatalytic capability of g-C_3N_4 to combine a-Fe_2O_3 and g-C_3N_4. Therefore, g-C_3N_4@a-Fe_2O_3 was prepared using a straightforward one-step approach in this study, and the activation of H_2O_2 as a heterogeneous catalyst was investigated. Particular attention was paid to how pH affected the coupled process (g-C_3N_4@a-Fe_2O_3/H_2O_2) Instead of the electrostatic attraction between the matrix and the catalyst as was previously postulated, the considerable impact of the solution's pH on the functionality and stability of g-C_3N_4@a-Fe_2O_3 may be mostly attributable to the leaching of iron ions. At last, catalyst's characterization and the experimental findings indicate that the g-C_3N_4@a-Fe_2O_3 mechanism of the activated H_2O_2 process is clearly understood. The activity of g-C_3N_4 supported by 15% a-Fe_2O_3 nanorods is raised by 3 times and 3.5 times when compared to pure g-C_3N_4 and pure a-Fe_2O_3 nanorods, respectively.Using various spectral methods, the excellent characteristics of the composite material a-Fe_2O_3@ g-C_3N_4 were obtained .

ISSN:2790-1688 DOI: 10.56028/aetr.2.1.443

2. Materials and methods

2.1 Materials.

Both bisphenol A (99%) and 5,5-dimethyl-1-pyrrolidine N-oxide (DMPO) were purchased from Aladdin in China. The analytical grade isopropyl alcohol (IPA), $Fe(NO_3)_3 \cdot 9H_2O$, NaOH, H_2SO_4, and urea were all purchased from Sinopharm Chemical Reagent Co. in China. Triethanolamine (TEOA) and zp-Benzoquinone (BQ) were supplied by Aladdin Ltd. (Shanghai, China). All of the materials utilized in the investigation were not deep purified, and Milli-Q water was used throughout.

2.2 Creation of g-C_3N_4.

By heating urea, graphitized carbon nitride (g-C_3N_4) was created[26]. Alumina crucible with a lid and 10 g of urea were used for the drying process, which took one hour at 80°C. The urea was subsequently heated to 520°C using a PID temperature controller in a reliable burner at a heating rate of 2.3°C/min1, and kept at this temperature for 3 hours. After waiting until it has reached room temperature, obtain a light yellow g-C_3N_4 3.

2.3 Hydrothermal synthesis of a-Fe_2O_3 nanorods

$Fe(NO_3)_3 \cdot 9H_2O$ diffluence was determined in 20 mL deionized water, and NaOH solution was added in with vigorous stirring to get pH to 12. The resultant solution was then hydrothermally treated at 180°C for 24 hours after being sealed in a Teflon autoclave. Centrifugation, washing in deionized water, and 24-hour drying at 60 °C

2.4 Hydrothermal synthesis of g-C_3N_4@a-Fe_2O_3 composites

To create a well-separated mono-layer of C_3N_4 in a classical experiment, the correct amount of g-C_3N_4 was dispersed in 50 mL of deionized water and processed sonographically for two hours in an ultrasonic bath. The previously prepared Fe_3+ precipitate was then added, and the yellow g-C_3N_4 suspension was agitated for 30 minutes. The technique for creating a-Fe_2O_3 nanorods after that is the same as what was previously stated. With values of 5, 10, 15, and 20 weight percent, different amounts of a-Fe_2O_3 were loaded onto g-C_3N_4.

2.5 Characterization

The Rigaku D/Max-Rb diffractometer was used to obtain powder X-ray diffraction (XRD) images of Cu-Ka radiation (λ=15418 a) in the 10-80º2θ range. In the spectral region of 200–800 nm, ultraviolet–visible proliferating reflectance (DRS) spectrum data were collected using a PerkinElmer λ 950 spectrophotometer at room temperature. Thermo Nicolet Avatar 370 FTIR spectrophotometer and the KBr pellet technique were used to determine the Fourier transform infrared spectrum. Perform scanning electron microscopy (SEM) and energy-dispersive X-ray spectra using a JEOL JEM-100C II electron microscope from Japan (EDX).

2.6 Experimental procedure and analyses

A UV filter (λ ⩾420 nm) and a 500 W halogen tungsten light were both employed as sources of visible light. And use a cylindrical glass container with a glass casing to house the light. Under visible light, bisphenol A was degraded by photoreactor. In each experimentation, a water based solution of BPA (0.4 g/ L) was positioned in the reactor and the desired catalytic dose was added. The levitation is then mixed with a constant speed magnetic force for 30 minutes, and the lamp is turned on while the required volume of H_2O_2 is put into the reaction kettle. To change the working solution's initial pH to the appropriate level, use HNO_3 or NaOH solution. The working settlement of the added material is mixed at room temperature with a magnetic stirrer for a preset period of time. The flow rate was $_1$ mL/min, the injection volume was 40 mL, and the analysis spectrum was

ISSN:2790-1688 DOI: 10.56028/aetr.2.1.443
278 nm. The flowing phase was a 70:30 mixture of methanol and water. To determine the pH of the fluid, a composite glass electrode was connected to a Mettler Toledo FE 20 pH meter. After combining 1,10-phenanthroline, an iron-phenanthroline complex is created. The amount of H_2O_2 present was determined using an iodimetry titration, and the iron ion's dipping volume was determined using a spectrophotometer at 510 nm. Jena Multi N/C 3100 TOC analyzer was used to detect residual TOC in the aqueous solutions. Spectra of electron spin resonance (ESR) are maintained below. When employing the ESP 300E electronic paramagnetic resonance spectrometer with a xenon lamp (420 nm filter) as an illumination source, the spin signal of free radicals caught by DMPO was obtained.

After many applications, the stability of photocatalyst was studied. After each photocatalytic reaction, clean the solid photocatalyst and dry it with deionized water to ensure it can be reused.

3. Results

3.1 XRD analysis

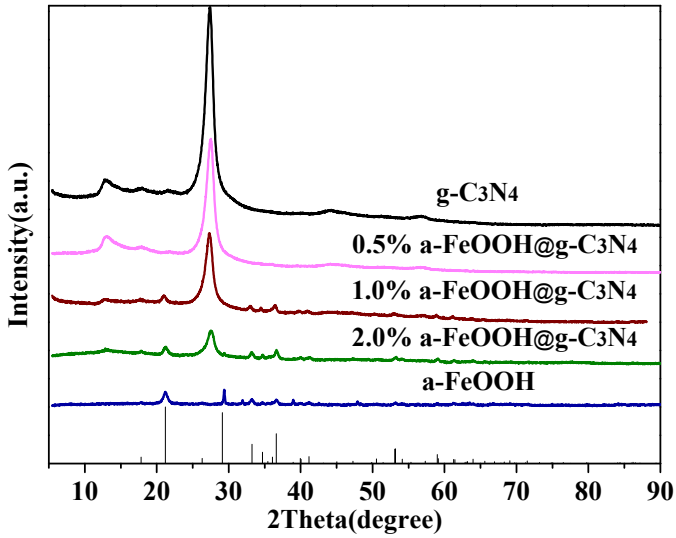

Fig. 1 XRD patterns of (a) pure a-Fe_2O_3, (b) pure g-C_3N_4, (c) 0.5% a-Fe_2O_3@C_3N_4, (d) 1.0% a-Fe_2O_3@C_3N_4 and (e) 2.0% a-Fe_2O_3@C_3N_4.

The structural features and elemental composition of pure a-Fe_2O_3 nanorods and a-Fe_2O_3 nanorods@g-C_3N_4 nanocomposites were confirmed by the XRD patterns (Fig. 1). The orthogonal a-Fe_2O_3 system in JCPDS document no. 81-0462 is related with the XRD peaks. There were no highly similar indexing surfaces or impurity correlation peaks to be seen. The produced photocatalyst exhibits a high purity of the crystal phase, and the relative widening of the reflection peak suggests the production of nanomaterials. For pure G-C_3N_4, what can be observed at 2θ= 27.4° is a strong diffraction peak, which is used as the diffraction plane (002) for graphite carbon nitride materials (JCPDS File No. 87-1526), famous as its melon nets27. On the (100) crystal plane of g-C_3N_4, there is another weak diffraction peak at 2θ= 13.1° that resembles the interplanar structural stacking of tris-triazine unit 28. The crystal phase of a-Fe_2O_3 and the crystal plane of g-C_3N_4 remain the same when joined to one another. Though the interfacial structure of tris-triazine unit 29 is disrupted by coupling and deposited in g-C_3N_4@a-Fe_2O_3, the diffraction peak of g-C_3N_4 at 2θ=13.1° vanishes. The mass fraction of a-Fe_2O_3 is inversely correlated with the a-Fe_2O_3 diffraction peak. Only the a-Fe_2O_3 and g-C_3N_4 phases were discovered in the composite since no other impurity peaks could be seen in the XRD pattern.

ISSN:2790-1688 DOI: 10.56028/aetr.2.1.443

3.2 UV-vis diffuse reflectance spectra

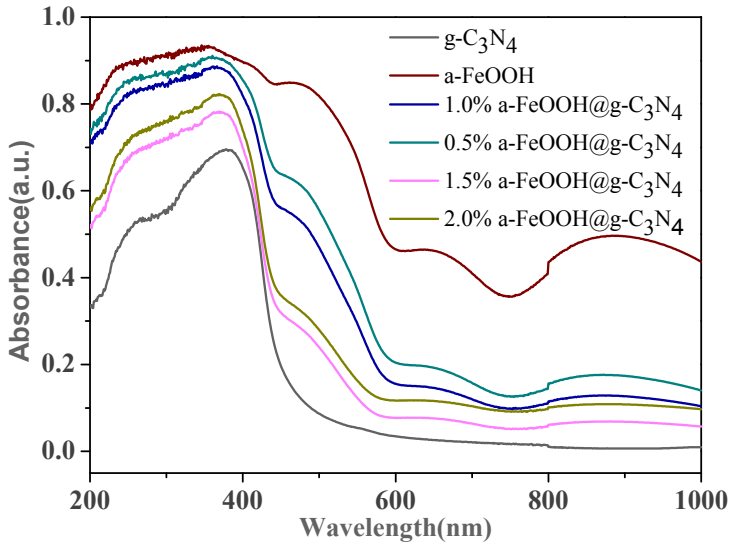

Fig. 2 UV-vis diffuse reflectance spectrum of a-Fe_2O_3@ g-C_3N_4 (a) pure g-C_3N_4, (b) 5% (c) 10% (d) 15% (e) 20% and (f) pure a-Fe_2O_3.

The equivalent DRS for the composite is displayed in Figure 2 to help with comprehension of the optic performance. All wavelength ranges of a-Fe_2O_3 range were examined. Additionally, because a-E_2O_3 has a larger absorption coefficient in the near-infrared region, the absorption of the composites at 600–800 nm is improved with an increase in a-Fe_2O_3 mass fraction.

3.3 TEM analysis

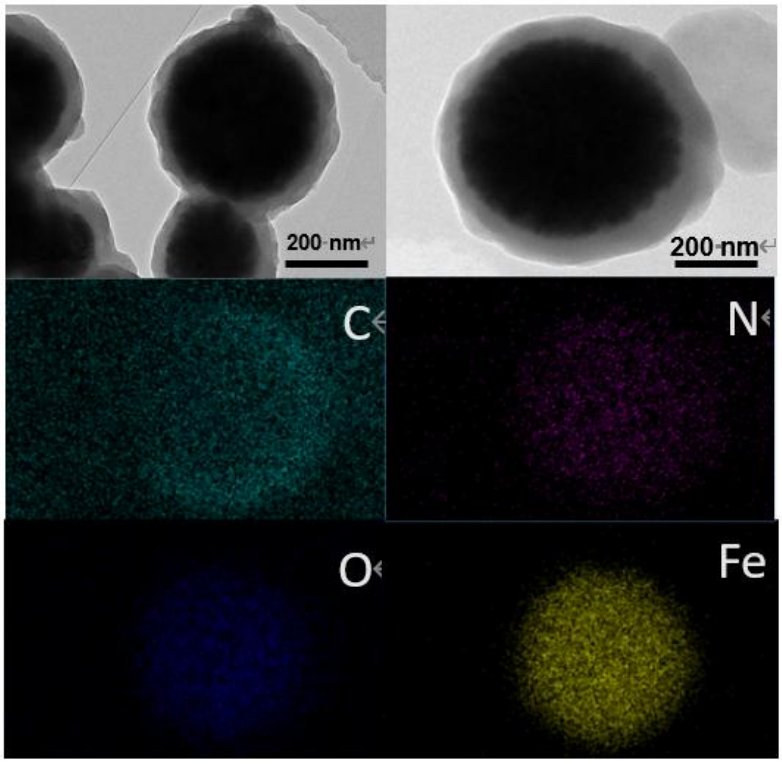

Fig. 3 (A) and (B) HRTEM; (C) mapping images of 15% a-Fe_2O_3@C_3N_4

The morphological properties of a-Fe_2O_3, bare g-C_3N_4, and 15% a-Fe_2O_3@C_3N_4 are shown in Figure 3. (Fig. 3A) show the canonical morphological characteristics of g-C_3N_4 composited by

ISSN:2790-1688 DOI: 10.56028/aetr.2.1.443
melamine polymerization43. Fig. 3B shows the SEM image of a-Fe_2O_3 microcrystals. As can be seen, many irregular nanorods self-assemble into rod-like upper Infrastructure. Fig. 3C show the morphology of 15% a-Fe_2O_3@C_3N_4. After g- combined with a-Fe_2O_3, the size of g-C_3N_4 particles tended to become homogeneous and the lamellar structure decreased. Moreover, rod-like microcrystals are composed of irregular nanorods themselves.

3.4 Performance of photo-Fenton photocatalysis

The photo-Fenton photocatalytic reaction of several catalysts was carried out under optical light treatment in the presence of H_2O_2 in order to access the activity of the g-C_3N_4@a-Fe_2O_3 composite, as shown in Fig. 4. H_2O_2 degradation and direct photodegradation of BPA (blank) under optical light might both be disregarded. Pure a-Fe_2O_3 has very little capacity to decompose when exposed to visible light without the aid of H_2O_2. However, the g-C_3N_4 conjugation affects its capacity for degradation. The findings demonstrate that, within a particular range, the mass fraction of a-Fe_2O_3 can enhance photocatalytic activity. The photocatalytic effect can be enhanced when the mass fraction of a-Fe_2O_3 is less than 15%, but when the mass fraction of a-Fe_2O_3 is increased to 20%, the degradation rate of BPA is lower than 15% of a-Fe_2O_3 composite material. Therefore, in this study, 15% a-Fe_2O_3 has the perfect photocatalytic viability. This may be because the surplus a-Fe_2O_{33} covering the surface provides a compound center for the electron-hole pair produced by light, thus preventing the effective utilization of optical light by g-C_3N_4. This will limit the contribution of g-C_3N_4 to the Fenton reaction of a-Fe_2O_3, which means the promoting effect of g- C_3N_4 on a-Fe_2O_3 Fenton reaction cannot be fully demonstrated. Therefore, it is necessary to control a certain amount of a-Fe_2O_3 in the composite catalyst to promote the photocatalytic efficiency of photo-Fenton.

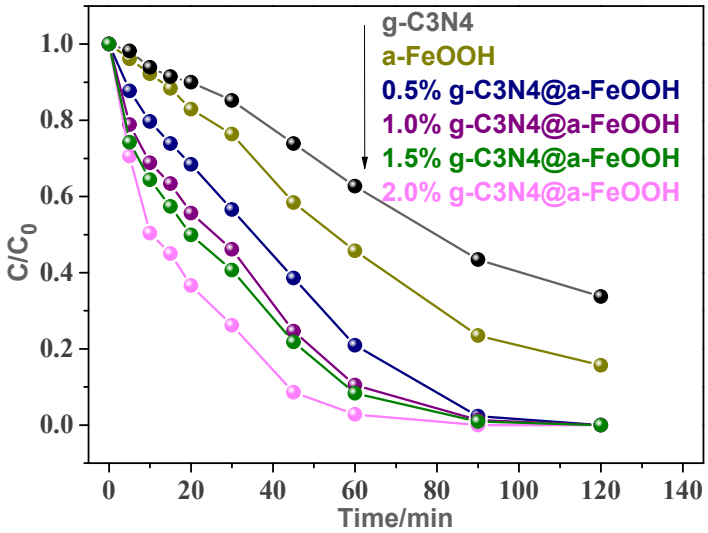

Fig. 4 BPA breakdown over the various catalysts when exposed to visible spectrum and H_2O_2.

3.5 Radical trapping experiments

We performed capture experiments to investigate the primary active components44 in order to further clarify the photo-Fenton photocatalytic mechanism. IPA which may absorb •OH radicals, dramatically lowers the catalytic activity of a-Fe_2O_3@C_3N_4 by 15%, as shown in Figure 5. The addition of triethanolamine (TEOA) also reduces the reaction rate and can capture the well. However, there was no discernible difference in the rate of degradation when the p-benzoquinone (BQ) scavenger was added. The photogenerated holes are the primary oxidizing agents in the photo phentonic photocatalytic process, according to the results of the capture experiment.

To support this finding, using EtOH—a radical scavenger for •OH and •SO_4, in an EPR experiment with DMPO acting as the radical search agent to look for any radical formation. As

ISSN:2790-1688 DOI: 10.56028/aetr.2.1.443
shown in Fig. 5, the addition of ethyl acetate induces the formation of DMPO-SO_4 and DMPO-OH adduct signals, which are then amplified by the addition of 15% a-Fe_2O_3@C_3N_4 (producing 15% Fe_2O_3@C_3N_4/H_2O_2/Vis processes). This observation can be likened to systems that have been brightened by visible light, which indicates that more free radicals are generating. The findings demonstrated that exposure to visible light can cause the free radicals •OH and •SO_4 37, which promotes BPA discoloration.

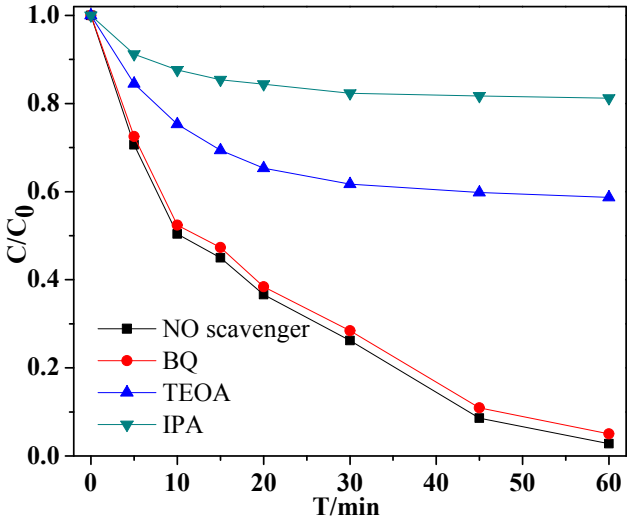

Fig. 5 Effect of the several scavengers on BPA decomposition exceeding 15% a-Fe_2O_3@C_3N_4 in presence of H_2O_2 under visible range radiation.

3.6 ESR analysis

To investigate the effect for the active species due to the coupling of a-Fe_2O_3 with the g-C_3N_4, ESR spin-trap experiments were carried out. To confirm this observation, we used EtOH, which is free radical scavenger •OH and •SO_4, and DMPO as free radical scavenger to inspect free radical formation in EPR experiments. Fig. 6 a shows that the H_2O_2/dark process did not investigate a significant signal confirming that BPA depigmentation of H_2O_2 alone was caused by a non-free radical reaction. The DMPO-OH adduct signal was muted when EtOH was introduced to the reaction system. In the procedure of H_2O_2/Vis, DMPO-OH adduct signals occurred, and the addition of 15% g-C_3N_4@a-Fe_2O_3 amplified these signals, demonstrating the formation of additional free radicals. These findings imply that exposure to visible light may cause the production of •OH 37 radicals and hence accelerate BPA discoloration. The signals for different composites are displayed in Fig. 6b. The signal strengths are in the range of 15% g-C_3N_4@ a-Fe_2O_3 > a-Fe_2O_3 > g-C_3N_4, which amplified the fact that the composite made of 15% g-C_3N_4@a-Fe_2O_3 was more effective at degrading the pollutants.

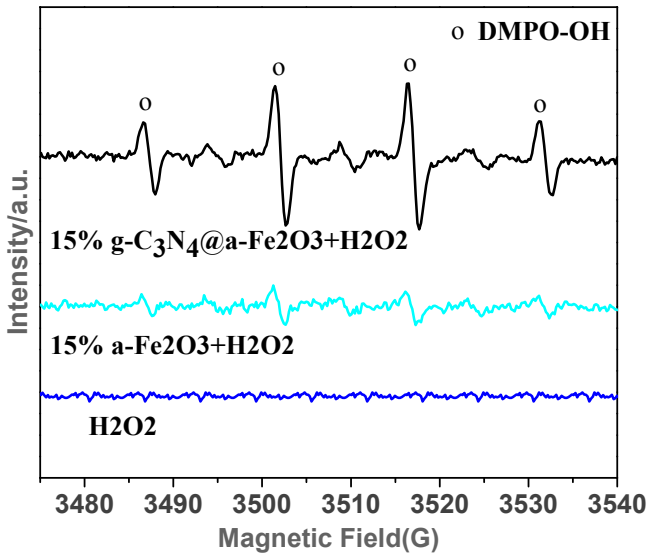

Fig. 6 Various processes' EPR spectra with and without BPA. g-C_3N_4@a-Fe_2O_3 (0.4 g/L), H_2O_2 (8.0 mmol/L), DMPO (18 mmol), starting pH 5.0, and photocatalytic reaction duration 5 min.

3.7 Electrochemistry analysis

The photocurrent reaction of pure g-C_3N_4 and composites made of 15% g-C_3N_4@a- Fe_2O_3 and a-Fe_2O_3 is shown in Fig. 7. When the light has been on, the current intensity is steady; when the light is out, it quickly returns to the electrically dark state. The photocurrent is created by isolating and sending the photoinduced charges to the active electrodes. When pure g-C_3N_4, a-Fe_2O_3, and 15% g-C_3N_4@a- Fe_2O_3 are compared for photocurrent intensity, it is discovered that the 15% g-C_3N_4@a- $Fe_2O_3$3 compound has a higher current than the pure g-C_3N_4 and a-Fe_2O_3. According to the findings, it is more effective at separating electrons and holes and has a longer carrier life than pure g-C_3N_4 and a-Fe_2O_3 (15 percent g-C_3N_4@a- Fe_2O_{33}).

EIS experiments were carried out in order to show how 15% g-C_3N_4@a- Fe_2O_3 composite outperformed pure g-C_3N_4 and a-Fe_2O_3 for charge carrier transfer. The 15 percent g-C_3N_4@a- Fe_2O_3 composite has a lower charge shift resistance and a more effective electron-hole pair isolation as seen by the smaller Nyquist circle trail of the compound than that of pure g-C_3N_4.

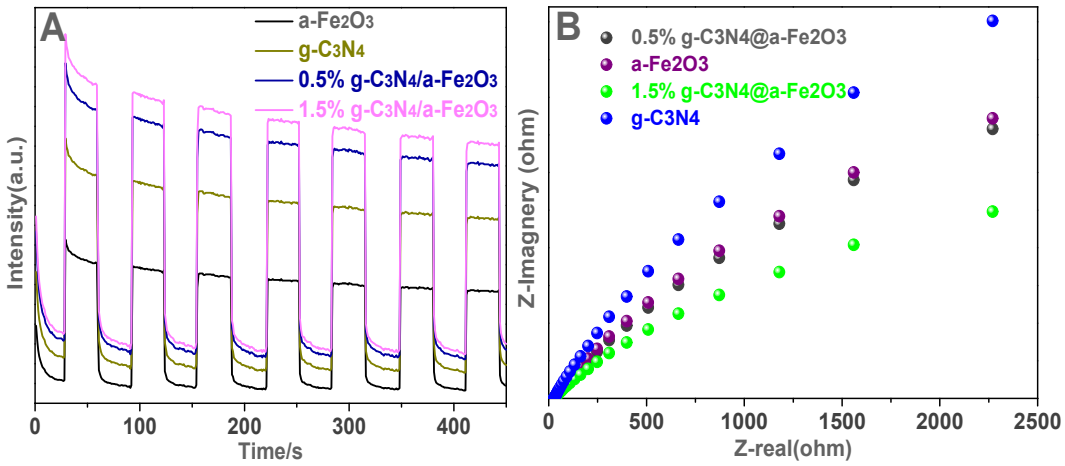

Fig. 7. (A) Transient photocurrent response of sample electrodes made from pure C_3N_4 and composites made of 15 weight percent g-C_3N_4@a-Fe_2O_3. (B) Nyquist plots of the sample electrodes of pure g-C_3N_4 and $_{15}$ weight percent g-C_3N_4@a-Fe_2O_3 composites from EIS.

ISSN:2790-1688 DOI: 10.56028/aetr.2.1.443

3.8 XPS analysis

XPS investigation was carried out to further evaluate the surface state and chemical make-up of iron at 15% g-C_3N_4@a-Fe_2O_3. In accordance with the EDX characterization, Fig. 8 a shows XPS examination spectrum at 15% g-C_3N_4@a-Fe_2O_3 indicates the presence of C, O, Fe, and N. The faulty sp2 hybrid carbon atoms on the pure graphite sites in the carbon-carbon domain and CN matrix are what cause the sp2 hybrid carbon atoms on the C-C, C=N, and C=O bonds to have the combination energies of C 1s at 284.7, 287.9, and 288.9 eV, respectively23, 24. The combination energies of N 1s are 398.3, 399.5, and 400.7 eV, which, respectively, correspond to sp2 hybrid N atoms in C=N, sp3 hybrid N atoms in C-[N]3, and C- NHX. Deeper dissections of high resolution XPS spectra were performed at around 720.0 eV in the Fe 2P area (Fig. 8b) and 532.0 eV in the O_1s area (Fig. 8c). According to Fig. 8b, the two peaks at 711.3 and 724.8 eV, respectively, are associated with the Fe 2p3/2 and Fe 2p1/2 core power levels, which is consistent with previously published findings on a-Fe_2O_3 (711.4 and 724.6 eV) 45. An oxidation state of Fe_3+ is present as evidenced by the 13.2 eV energy gap between the spin orbital dipoles. 46 Additionally, the satellite's peak at 719.1 eV provides additional evidence that Fe_3+ species are present on $_{15}$% of the surface of g-C_3N_4@a-Fe_2O_3. The high-resolution O1s spectra exhibited in Fig. 8c after the curve has been adjusted shows two peaks at 529.6 eV and 530.9 eV, which represent, respectively, C=O and sp_2-hybridized O atoms in the oxygen of the a-Fe_2O_3 lattice45, 47. The results support the conclusion that a-Fe_2O_3 has been successfully loaded onto g-C_3N_4 by SEM, EDX and XRD.

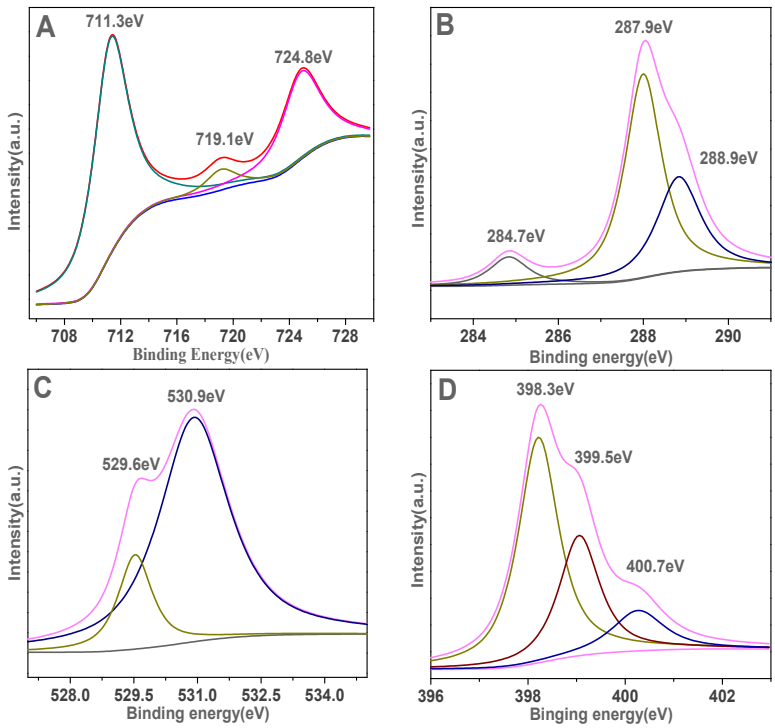

Fig. 8. XPS spectrum of the 15% g-C_3N_4@a-Fe_2O_3 composites: Fe 2p (A), C 1s(B), N 1s(C), O 1s(D).

3.9 The regime of photo-Fenton catalytic reaction of g-C_3N_4@a-Fe_2O_3 composite was presented

The formation of active •OH and •SO_4 species was confirmed by DMPO's ESR rotary pitfall technique. DMPO functions as a stable DMPO/ $O^{2\bullet-}$ or DMPO/•OH radical scavenger in general. Image displays a four-line spectrum with compared strength of 1:2:2:1 under visible light exposure, which we believe is the properties spectrum of DMPO/•OH and DMPO/•SO_4 adduct 48. On the

ISSN:2790-1688 DOI: 10.56028/aetr.2.1.443
contrary, when the situation is dark environment, we cannot investigate significant ESR signal. In addition, no DMPO/ •OH signal was inspected under dark and visible light irradiation. It also displays that •OH is the major oxidizing lively matter.

Since IFCT is a surface phenomenon, so the number of excited electrons produced by light absorption is limited, so the excited electrons generated by g-C_3N_4 can be separated into two categories after being exposed to visible light. The first kind of electron has the ability to enter transmission of G-C_3N_4 zone and unite with dispersed $S_2O_8^{2-}$ to create $\bullet SO_4$; But because of the huge energy level difference and ease of the synthesis of •OH, the CB electron of g-C_3N_4 (−1.23V) cannot move energy to Fe (III) (0.77V). Interfacial charge transfer (IFCT) induced by visible light is the second sort of electrons produced by light in the g-C_3N_4 price band49, 50, while the pores continue to be within the g-C_3N_4 pricing range. This reduces the distance over which electrons must travel, making it simple to swiftly separate photogenerated holes from electrons, increasing the mobility of the holes and expanding the region of visible light absorption. Being unstable, Fe(II) is readily transformed to Fe(III) by persulfate in the presence of environmental factors, suggesting that Fe(III) is recycled and Fe(III)/Fe(II) maintains a dynamic equilibrium of H_2O_2. Oxygen ($S_2O_8^{2-}$) is converted to$\bullet SO_4$ ($S_2O_8^{2-} + Fe(II) \rightarrow Fe(III) + \bullet SO_4 + SO_4^{2-}, \bullet SO_4 + H_2O \rightarrow \bullet OH^+ + SO_4^{2-}$)48. Fe (III)/Fe (II) can accomplish the multi-electron reduction of oxygen and enhance the electron transport, which improves the photocatalytic activity in comparison to the single-electron reduction of CB in g-C_3N_4. In addition, compared with the active substance of mild oxidant $\bullet SO_4$, the pores in C_3N_4 VB showed strong photooxidation ability, which made BPA have good mineralization51 . In contrast, although holes are involved in photocatalytic reactions, as mentioned above, holes are also involved in other reactions.

Therefore, photodegraded BPA is not thoroughly transformed to CO_2. Thus, Combining the above factors, fast charge transfer improves carrier isolation by leaving pores in C_3N_4 and Fe (III) BB, allowing IFCT to produce more efficient electrons to reduce oxygen, resulting in the optimal photocatalytic performance of 15% a-Fe_2O_3@C_3N_4 composites. Through the coupling of C_3N_4 and a-Fe_2O, the distribution of a-Fe_2O in the composite is good, the size is small, and the content is high, so the composite has more active sites than a single material. As a result, ternary photocatalysts have higher light intake and less charge reorganization, bringing about better photocatalytic activity.

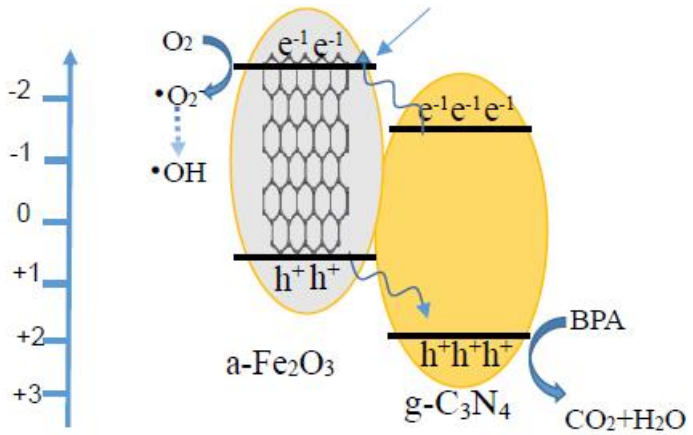

Fig. 9 Proposed photo-Fenton photocatalytic reaction mechanism for 15% a-Fe_2O_3/g-C_3N_4 composites

4. Conclusions

In conclusion, I successfully used the hydrothermal approach to create the unique g-C_3N_4@a-Fe_2O_3 spheres with various g-C_3N_4 mass percents. Due to the interaction with the

ISSN:2790-1688 DOI: 10.56028/aetr.2.1.443
g-C_3N_4 photocatalyst, the catalytic activity of Fenton's reagent a-Fe_2O_3/H_2O_2 under visible light and no-light irradiation is greatly increased. The g-C_3N_4@a-Fe_2O_3 microspheres exhibit improved photocatalytic viability due to up visible light sensitivity and katabatic reorganization of photoinduced vectors. Besides, g-C_3N_4@a-Fe_2O_3 spheres are extremely steady and reusable in photo-Fenton photocatalytic reactions. It was suggested that the photo-Fenton photocatalytic reaction of g-C_3N_4@a-Fe_2O_3 spheres was the mechanism used to explain the synergistic impact of a-Fe_2O_3 and g-C_3N_4. The findings demonstrate that g-C_3N_4@a-Fe_2O_3 microspheres, a novel form of photocatalyst, can consistently remove non-biodegradable organic contaminants in wastewater.

Acknowledgements

This work was supported by the Fundamental Research Funds for the Central Universities (2018B53314) and Financial supported by National Natural Science Foundation of China (No. 51708543 and No. 51738013). Special thanks to the Key Laboratory of Integrated Regulation and Resource Development on Shallow Lakes for its support of this research work.

Reference

[1] Levine, A. D.; Asano, T., Peer reviewed: recovering sustainable water from wastewater. Environmental science & technology 2004, 38, (11), 201A-208A.

[2] Tsitonaki, A.; Petri, B.; Crimi, M.; Mosbæk, H.; Siegrist, R. L.; Bjerg, P. L., In situ chemical oxidation of contaminated soil and groundwater using persulfate: a review. Critical Reviews in Environmental Science and Technology 2010, 40, (1), 55-91.

[3] Antonopoulou, M.; Evgenidou, E.; Lambropoulou, D.; Konstantinou, I., A review on advanced oxidation processes for the removal of taste and odor compounds from aqueous media. Water research 2014, 53, 215-234.

[4] Xiang, L.; Royer, S.; Zhang, H.; Tatibouët, J.-M.; Barrault, J.; Valange, S., Properties of iron-based mesoporous silica for the CWPO of phenol: A comparison between impregnation and co-condensation routes. Journal of hazardous materials 2009, 172, (2), 1175-1184.

[5] Yao, Y.; Cai, Y.; Lu, F.; Qin, J.; Wei, F.; Xu, C.; Wang, S., Magnetic $ZnFe_2O_4$–C_3N_4 hybrid for photocatalytic degradation of aqueous organic pollutants by visible light. Industrial & Engineering Chemistry Research 2014, 53, (44), 17294-17302.

[6] Zhao, Z.; Sun, Y.; Dong, F., Graphitic carbon nitride based nanocomposites: a review. Nanoscale 2015, 7, (1), 15-37.

[7] Wang, X.; Maeda, K.; Thomas, A.; Takanabe, K.; Xin, G.; Carlsson, J. M.; Domen, K.; Antonietti, M., A metal-free polymeric photocatalyst for hydrogen production from water under visible light. Nature materials 2009, 8, (1), 76-80.

[8] Li, M.; Pokhrel, S.; Jin, X.; Mädler, L.; Damoiseaux, R.; Hoek, E. M., Stability, bioavailability, and bacterial toxicity of ZnO and iron-doped ZnO nanoparticles in aquatic media. Environmental science & technology 2010, 45, (2), 755-761.

[9] Wang, X.; Maeda, K.; Chen, X.; Takanabe, K.; Domen, K.; Hou, Y.; Fu, X.; Antonietti, M., Polymer semiconductors for artificial photosynthesis: hydrogen evolution by mesoporous graphitic carbon nitride with visible light. Journal of the American Chemical Society 2009, 131, (5), 1680-1681.

[10] Dong, G.; Zhao, K.; Zhang, L., Carbon self-doping induced high electronic conductivity and photoreactivity of gC_3N_4. Chemical Communications 2012, 48, (49), 6178-6180.

[11] Zhang, X.-S.; Hu, J.-Y.; Jiang, H., Facile modification of a graphitic carbon nitride catalyst to improve its photoreactivity under visible light irradiation. Chemical Engineering Journal 2014, 256, 230-237.

[12] Wang, Y.; Wang, X.; Antonietti, M., Polymeric graphitic carbon nitride as a heterogeneous organocatalyst: from photochemistry to multipurpose catalysis to sustainable chemistry. Angewandte Chemie International Edition 2012, 51, (1), 68-89.

ISSN:2790-1688 DOI: 10.56028/aetr.2.1.443
[13] Deguillaume, L.; Leriche, M.; Desboeufs, K.; Mailhot, G.; George, C.; Chaumerliac, N., Transition metals in atmospheric liquid phases: Sources, reactivity, and sensitive parameters. Chemical Reviews 2005, 105, (9), 3388-3431.

[14] Zhang, G.; Wang, S.; Yang, F., Efficient adsorption and combined heterogeneous/homogeneous Fenton oxidation of amaranth using supported nano-FeOOH as cathodic catalysts. The Journal of Physical Chemistry C 2012, 116, (5), 3623-3634.

[15] Li, H.; Li, W.; Zhang, Y.; Wang, T.; Wang, B.; Xu, W.; Jiang, L.; Song, W.; Shu, C.; Wang, C., Chrysanthemum-like α-FeOOH microspheres produced by a simple green method and their outstanding ability in heavy metal ion removal. Journal of Materials Chemistry 2011, 21, (22), 7878-7881.

[16] Adhyapak, P. V.; Mulik, U. P.; Amalnerkar, D. P.; Mulla, I. S., Low Temperature Synthesis of Needle ‐like α ‐FeOOH and Their Conversion into α ‐Fe_2O_3 Nanorods for Humidity Sensing Application. Journal of the American Ceramic Society 2013, 96, (3), 731-735.

[17] Zhou, X.; Yang, H.; Wang, C.; Mao, X.; Wang, Y.; Yang, Y.; Liu, G., Visible Light Induced Photocatalytic Degradation of Rhodamine B on One-Dimensional Iron Oxide Particles†. The Journal of Physical Chemistry C 2010, 114, (40), 17051-17061.

[18] Hojamberdiev, M.; Zhu, G.; Eminov, A.; Okada, K., Template-Free Hydrothermal Synthesis of Hollow α-FeOOH Urchin-Like Spheres and Their Conversion to α-Fe_2O_3 Under Low-Temperature Thermal Treatment in Air. Journal of Cluster Science 2013, 24, (1), 97-106.

[19] Kakuta, S.; Numata, T.; Okayama, T., Shape effects of goethite particles on their photocatalytic activity in the decomposition of acetaldehyde. Catalysis Science & Technology 2014, 4, (1), 164-169.

[20] Tonda, S.; Kumar, S.; Kandula, S.; Shanker, V., Fe-doped and-mediated graphitic carbon nitride nanosheets for enhanced photocatalytic performance under natural sunlight. Journal of Materials Chemistry A 2014, 2, (19), 6772-6780.

[21] Su, F.; Mathew, S. C.; Lipner, G.; Fu, X.; Antonietti, M.; Blechert, S.; Wang, X., mpg-C_3N_4-catalyzed selective oxidation of alcohols using O_2 and visible light. Journal of the American Chemical Society 2010, 132, (46), 16299-16301.

[22] Huang, L.; Xu, H.; Li, Y.; Li, H.; Cheng, X.; Xia, J.; Xu, Y.; Cai, G., Visible-light-induced WO_3/gC_3N_4 composites with enhanced photocatalytic activity. Dalton Transactions 2013, 42, (24), 8606-8616.

[23] Bai, S.; Wang, X.; Hu, C.; Xie, M.; Jiang, J.; Xiong, Y., Two-dimensional gC_3 N_4: an ideal platform for examining facet selectivity of metal co-catalysts in photocatalysis. Chemical Communications 2014, 50, (46), 6094-6097.

[24] Di, Y.; Wang, X.; Thomas, A.; Antonietti, M., Making Metal Carbon Nitride Heterojunctions for Improved Photocatalytic Hydrogen Evolution with Visible Light. ChemCatChem 2010, 2, (7), 834-838.

[25] Sun, J.; Zhang, J.; Zhang, M.; Antonietti, M.; Fu, X.; Wang, X., Bioinspired hollow semiconductor nanospheres as photosynthetic nanoparticles. Nature Communications 2012, 1139.

[26] Zhao, Y.; Shu, P.; Zhang, Y.; Lin, L.; Zhou, H.; Xu, Z.; Suo, D.; Xie, A.; Jin, X., Effect of Centella asiatica on oxidative stress and lipid metabolism in hyperlipidemic animal models. Oxidative medicine and cellular longevity 2014, 2014.

[27] Zheng, Y.; Lin, L.; Ye, X.; Guo, F.; Wang, X., Helical graphitic carbon nitrides with photocatalytic and optical activities. Angewandte Chemie International Edition 2014, 53, (44), 11926-11930.

[28] Hu, S.; Jin, R.; Lu, G.; Liu, D.; Gui, J., The properties and photocatalytic performance comparison of Fe_3+-doped gC_3 N_4 and Fe_2O_3/gC_3 N_4 composite catalysts. RSC Advances 2014, 4, (47), 24863-24869.

[29] Theerthagiri, J.; Senthil, R.; Priya, A.; Madhavan, J.; Michael, R.; Ashokkumar, M., Photocatalytic and photoelectrochemical studies of visible-light active α-Fe_2O_3–gC_3N_4 nanocomposites. RSC Advances 2014, 4, (72), 38222-38229.

[30] Fu, J.; Chang, B.; Tian, Y.; Xi, F.; Dong, X., Novel C_3N_4–CdS composite photocatalysts with organic–inorganic heterojunctions: in situ synthesis, exceptional activity, high stability and photocatalytic mechanism. Journal of Materials Chemistry A 2013, 1, (9), 3083-3090.

[31] Hou, Y.; Laursen, A. B.; Zhang, J.; Zhang, G.; Zhu, Y.; Wang, X.; Dahl, S.; Chorkendorff, I., Layered Nanojunctions for Hydrogen ‐ Evolution Catalysis. Angewandte Chemie International Edition 2013, 52, (13), 3621-3625.

ISSN:2790-1688 DOI: 10.56028/aetr.2.1.443
[32] Katsumata, K.-i.; Motoyoshi, R.; Matsushita, N.; Okada, K., Preparation of graphitic carbon nitride (gC_3N_4)/WO_3 composites and enhanced visible-light-driven photodegradation of acetaldehyde gas. Journal of hazardous materials 2013, 260, 475-482.

[33] Ye, X.; Cui, Y.; Qiu, X.; Wang, X., Selective oxidation of benzene to phenol by Fe-CN/TS-$_1$ catalysts under visible light irradiation. Applied Catalysis B: Environmental 2014, 152, 383-389.

[34] Ye, X.; Cui, Y.; Wang, X., Ferrocene‐Modified Carbon Nitride for Direct Oxidation of Benzene to Phenol with Visible Light. ChemSusChem 2014, 7, (3), 738-742.

[35] Gu, Q.; Gao, Z.; Zhao, H.; Lou, Z.; Liao, Y.; Xue, C., Temperature-controlled morphology evolution of graphitic carbon nitride nanostructures and their photocatalytic activities under visible light. RSC Advances 2015, 5, (61), 49317-49325.

[36] Liao, Y.; Zhu, S.; Ma, J.; Sun, Z.; Yin, C.; Zhu, C.; Lou, X.; Zhang, D., Tailoring the Morphology of g‐C_3N_4 by Self‐Assembly towards High Photocatalytic Performance. ChemCatChem 2014, 6, (12), 3419-3425.

[37] Mao, J.; Peng, T.; Zhang, X.; Li, K.; Ye, L.; Zan, L., Effect of graphitic carbon nitride microstructures on the activity and selectivity of photocatalytic CO_2 reduction under visible light. Catalysis Science & Technology 2013, 3, (5), 1253-1260.

[38] Ye, S.; Qiu, L.-G.; Yuan, Y.-P.; Zhu, Y.-J.; Xia, J.; Zhu, J.-F., Facile fabrication of magnetically separable graphitic carbon nitride photocatalysts with enhanced photocatalytic activity under visible light. Journal of Materials Chemistry A 2013, 1, (9), 3008-3015.

[39] Zhang, S.; Yang, Y.; Guo, Y.; Guo, W.; Wang, M.; Guo, Y.; Huo, M., Preparation and enhanced visible-light photocatalytic activity of graphitic carbon nitride/bismuth niobate heterojunctions. Journal of hazardous materials 2013, 261, 235-245.

[40] Li, M.; Zhang, L.; Fan, X.; Zhou, Y.; Wu, M.; Shi, J., Highly selective CO_2 photoreduction to CO over gC_3N_4/Bi_2WO_6 composites under visible light. Journal of Materials Chemistry A 2015, 3, (9), 5189-5196.

[41] Tan, C.; Gao, N.; Deng, Y.; An, N.; Deng, J., Heat-activated persulfate oxidation of diuron in water. Chemical engineering journal 2012, 203, 294-300.

[42] Mahdi-Ahmed, M.; Chiron, S., Ciprofloxacin oxidation by UV-C activated peroxymonosulfate in wastewater. Journal of hazardous materials 2014, 265, 41-46.

[43] Anipsitakis, G. P.; Dionysiou, D. D., Radical generation by the interaction of transition metals with common oxidants. Environmental science & technology 2004, 38, (13), 3705-3712.

[44] Huang, Y.-F.; Huang, Y.-H., Identification of produced powerful radicals involved in the mineralization of bisphenol A using a novel UV-$Na_2S_2O_8$/H_2O_2-Fe (II, III) two-stage oxidation process. Journal of Hazardous Materials 2009, 162, (2), 1211-1216.

[45] Liang, C.; Bruell, C. J.; Marley, M. C.; Sperry, K. L., Persulfate oxidation for in situ remediation of TCE. I. Activated by ferrous ion with and without a persulfate–thiosulfate redox couple. Chemosphere 2004, 55, (9), 1213-1223.

[46] Xu, X.-R.; Li, X.-Z., Degradation of azo dye Orange G in aqueous solutions by persulfate with ferrous ion. Separation and purification technology 2010, 72, (1), 105-111.

[47] Rodriguez, S.; Vasquez, L.; Costa, D.; Romero, A.; Santos, A., Oxidation of Orange G by persulfate activated by Fe (II), Fe (III) and zero valent iron (ZVI). Chemosphere 2014, 101, 86-92.

[48] Lei, Y.; Chen, C.-S.; Tu, Y.-J.; Huang, Y.-H.; Zhang, H., Heterogeneous Degradation of Organic Pollutants by Persulfate Activated by CuO-Fe_3O_4: Mechanism, Stability, and Effects of pH and Bicarbonate Ions. Environmental science & technology 2015, 49, (11), 6838-6845.

[49] Chen, C.; Zhou, Y.; Wang, N.; Cheng, L.; Ding, H., $Cu_2(OH)PO_4$/gC_3N_4 composite as an efficient visible light-activated photo-Fenton photocatalyst. RSC Advances 2015, 5, (116), 95523-95531.

[50] Padhi, D. K.; Parida, K., Facile fabrication of α-FeOOH nanorod/RGO composite: a robust photocatalyst for reduction of Cr (vi) under visible light irradiation. Journal of Materials Chemistry A 2014, 2, (26), 10300-10312.

ISSN:2790-1688 DOI: 10.56028/aetr.2.1.443
[51] Wang, S.; Wang, L.; Yang, T.; Liu, X.; Zhang, J.; Zhu, B.; Zhang, S.; Huang, W.; Wu, S., Porous α-Fe_2O_3 hollow microspheres and their application for acetone sensor. Journal of Solid State Chemistry 2010, 183, (12), 2869-2876.

[52] Xiao, D.; Dai, K.; Qu, Y.; Yin, Y.; Chen, H., Hydrothermal synthesis of α-Fe_2O_3/gC_3N_4 composite and its efficient photocatalytic reduction of Cr (VI) under visible light. Applied Surface Science 2015, 358, 181-187.

[53] Gao, Y.; Zhang, Z.; Li, S.; Liu, J.; Yao, L.; Li, Y.; Zhang, H., Insights into the mechanism of heterogeneous activation of persulfate with a clay/iron-based catalyst under visible LED light irradiation. Applied Catalysis B Environmental 2016, 185, (1), 22-30.

[54] Liu, M.; Qiu, X.; Miyauchi, M.; Hashimoto, K., Energy-level matching of Fe(III) ions grafted at surface and doped in bulk for efficient visible-light photocatalysts. Journal of the American Chemical Society 2013, 135, (27), 10064-10072.

[55] Nishikawa, M.; Mitani, Y.; Nosaka, Y., Photocatalytic Reaction Mechanism of Fe(III)-Grafted TiO_2 Studied by Means of ESR Spectroscopy and Chemiluminescence Photometry. Journal of Physical Chemistry C 2012, 116, (28), 14900-14907.

[56] Hu, J. Y.; Ke, T.; Hong, J., Improvement of phenol photodegradation efficiency by a combined g-C_3N_4 /Fe(III)/persulfate system. Chemosphere 2016, 148, 34-40.